NASA TECHNICAL NOTE

NASA TN D-4513

AN EXPLANATION OF ANOMALOUS NON-HOOKEAN DEFORMATION OF IONIC SINGLE CRYSTALS

by James P. Cusick and Donald R. Behrendt

Lewis Research Center
Cleveland, Ohio

NATIONAL AERONAUTICS AND SPACE ADMINISTRATION • WASHINGTON, D. C. • MAY 1968

AN EXPLANATION OF ANOMALOUS NON-HOOKEAN DEFORMATION OF IONIC SINGLE CRYSTALS

By James P. Cusick and Donald R. Behrendt

Lewis Research Center
Cleveland, Ohio

NATIONAL AERONAUTICS AND SPACE ADMINISTRATION

For sale by the Clearinghouse for Federal Scientific and Technical Information
Springfield, Virginia 22151 – CFSTI price $3.00

AN EXPLANATION OF ANOMALOUS NON-HOOKEAN DEFORMATION OF IONIC SINGLE CRYSTALS

by James P. Cusick and Donald R. Behrendt

Lewis Research Center

SUMMARY

Previously published non-Hookean load-deflection data are reviewed. The results of this review show that roughness of the sample loading surfaces contributes to the measured deflection. Simple calculations presented herein show the effect of surface roughness on load-deflection data. Experiments are described in which two simultaneous deflection measurements are made; one measures bulk sample deflections only, the other measures bulk and loading surface deflections. Non-Hookean effects are observed only when surface deflections are included in the measurement. Finally, microscopic surface examination reveals surface roughness of the size needed to produce the non-Hookean effect. The non-Hookean effects are a consequence of the experimental techniques and do not reflect the bulk properties of the sample.

INTRODUCTION

Non-Hookean load-deflection data for single crystals of sodium chloride (NaCl), lithium fluoride (LiF), and magnesium oxide (MgO) were first reported in 1959 by Stearns, Pack, and Lad (ref. 1): The initial portion of the load-deflection curve for compression and four-point bending departed from Hook's law. The load-deflection curves displayed a concave upward initial region followed by a concave downward portion which was considered to be macroyield. Drawing the steepest straight line through the measured data (i.e., a line corresponding to the maximum slope of the load-deflection curve) defines a "foot length" as the deflection observed between the beginning of loading and the intercept of this straight line with deflection axis. The foot length was reported to be dependent on specimen pretreatments such as annealing, water polishing, X-irradiation, and quenching. The experimental results were interpreted (ref. 2) as arising from dislocation processes in the bulk of the sample. These processes include dislocation pinning,

expansion of dislocation loops, and a high mobility associated with cleaved-in dislocations.

A report of more recent compression experiments by Stearns and Gotsky (ref. 3) describes a "refined apparatus possessing microstrain sensitivity." Non-Hookean stress-strain behavior was observed by means of this apparatus for ionic single crystals. The non-Hookean behavior was reported to be dependent on specimen pretreatment, rate of testing, and prestress. These results were also interpreted in terms of bulk dislocation processes. Stearns and Gotsky stated that their results established that the previously reported shape of the stress-strain curve (ref. 1) was indeed characteristic of the material under test.

Bending experiments on polycrystalline NaCl and MgO were reported by May, Grimes and Lad (ref. 4). These data also show a foot in the load-deflection curve; no interpretation was given.

The purpose of this report is to demonstrate by a theoretical analysis and by an experimental method that the non-Hookean stress strain behavior of the type reported in references 1 to 4 is a consequence of the experimental method used by these investigators and that within the limits of error of our experimental method the load deflection behavior of NaCl, KBr, KCl, and LiF is conventional and shows no foot character whatsoever.

PRELIMINARY CONSIDERATIONS

Several aspects of the results of references 1 to 4 have led to the reexamination of the phenomenon. The result of the review strongly suggests that an experimental problem is responsible for the anomalous effects, namely, roughness of sample loading surfaces. In this section the experimental methods of references 1 and 3 are reviewed, and representative load-deflection curves presented. A brief description of surface roughness concludes the section.

In the original experiments by Stearns, Pack, and Lad, the sample was placed on the load-cell table of the testing machine and was loaded by a machined bar that was rigidly attached to the movable crosshead of the testing machine. The load signal was recorded on a strip-chart recorder. From the known value of the crosshead velocity, the time axis of the strip chart was converted into a deflection axis. Figure 1 shows the initial portion of the load-deflection curve for quenched NaCl. The measured deflection includes sample deflection, sample-metal surface roughness deflections, testing machine deflections, and load-cell deflections. The authors corrected the measured data for load-cell deflections only.

The experimental apparatus of Stearns and Gotsky is shown in figure 2. Deflections were measured by means of a lever beam; one end of the beam supported an LVDT core,

and the other end was fitted with a probe that rested inside a slot cut into the tungsten carbide loading anvil. A representative load-deflection curve is shown in figure 3. The measured deflection contained the deflections of the sample-metal loading surfaces as well as sample deflections. Thus, surface roughness of the sample, load-cell table, and loading anvil were all included in the measured deflection. Stearns and Gotsky give the measured deflection without corrections for surface roughness.

Since the experimental methods of references 1 and 3 measure surface roughness, consider the magnitude of surface roughness to be expected from the sample preparation methods which were reported. In the original experiments of Stearns,. Pack, and Lad, loading surfaces were cleaved surfaces. Consequently, the sample loading surfaces may be expected to have steps, cleavage damage, or other irregularities with heights ranging from a few to perhaps several hundred microinches (10^{-2} to 1 μm).

Stearns and Gotsky describe a surface preparation method which consists of grinding the sample loading faces on emery polishing paper. The final lapping was performed with 4/0 paper. Grinding was done dry with a glass plate backing for the polishing paper. Stearns and Gotsky report the surface finish obtained by this method was 4 microinches (0.01 μm) rms as determined by "interferometric" methods.

Many factors contribute to the final surface roughness of any polishing method. As for the Stearns-Gotsky method, the following factors should be important: (1) the grit size, (2) the relative hardness of grit and sample material, (3) the abrasive quality of the pulverized sample material which lies in the grit, (4) the cleaning method employed after polishing, (5) the airborne contamination, and (6) the atmospheric water vapor effects on polished surfaces. Of these, perhaps grit size is the most important. The 4/0 emery polishing paper used for final lapping has a grit size of about 15 microns. If one assumes a spherical grit geometry, the final lapping was done with emery particles greater than 500 microinches (12.7 μm) in diameter. Pulverized sample material in the grit would tend to reduce the size of emery particles exposed to the sample surface. It is difficult to believe that this method would consistently produce NaCl surfaces with a 4 microinch (0.01 μm) rms finish.

In a subsequent section crystal surfaces prepared in various ways will be examined. The interference microscope will be shown to be inadequate for defining an rms surface roughness for NaCl surfaces prepared by the Stearns-Gotsky method.

ANALYSIS SECTION

The shape of the load-deflection curve which would be obtained from an ideal elastic solid with surface roughness is now considered. The experimental arrangement to be analyzed is shown in figure 4. For simplicity, all roughness is assumed to exist on one

sample surface. Parameters associated with the surface roughness will be designated by the subscript S, and parameters associated with the bulk properties of the sample by the subscript B. A sample material which is perfectly elastic for any stress σ in the range $0 \leq \sigma \leq \sigma_Y$ where σ_Y is the yield stress is assumed, and the material is to deform plastically at $\sigma \geq \sigma_Y$ with a negligible work hardening.

The sample has a height h_B and a uniform cross section A_B (see fig. 4). The sample ends are flat and parallel. On the top surface of the sample is constructed a roughness region of height h_S. A flat and nondeformable plate is used to apply a load to the sample. The distance of the loading plate from the sample base is given by x_P. The loading plate contacts the highest point of the roughness region when $x_P = h_B + h_S$. At any applied load L the sample bulk and surface roughness both deform so that the total "measured" deflection D_T is given by

$$D_T = D_B + D_S = h_B + h_S - x_P \tag{1}$$

where D_B and D_S are the deflections of the bulk and surface, respectively. The deflection of the bulk portion of the sample can be expressed in terms of the applied load L and the Young's modulus Y as

$$D_B = Lh_B/YA_B \qquad 0 \leq L \leq L_{max} \tag{2a}$$

where

$$L_{max} = \sigma_Y A_B \tag{2b}$$

The surface roughness is now considered in more detail. A convenient way of describing the surface roughness is to define a function A_S to be the area of contact between the roughness region and the loading plate; A_S is specified to be a function of a measured distance above an arbitrary base plane. The base plane is chosen as the horizontal surface through the sample above which the cross-sectional area is less than A_B. An upward directed distance is represented by the variable x_S. Thus,

$$x_S = x_P + D_B - h_B \tag{3a}$$

and

$$A_S = A_S(x_S) \tag{3b}$$

such that

$$A_S(0) = A_B$$

and

$$A_S(x_S \geq h_S) = 0$$

The deformation of the surface roughness is assumed to be as follows. As the sample is loaded in compression, the surface roughness is deformed so that the area of roughness in contact with the loading plate is given by L/σ_Y. Consequently, for this model the load-deflection properties of the surface roughness region are obtained from the relation

$$L = \sigma_Y A_S \tag{4}$$

where L and A_S are functions of x_S. When the form of the area function A_S is specified, the deflection of the surface roughness can be calculated in terms of applied load.

An area function is now considered which decreases linearly with x_S. Thus,

$$A_S = A_B\left(1 - \frac{x_S}{h_S}\right) \qquad 0 \leq x_S \leq h_S \tag{5}$$

From equations (2b), (4), and (5)

$$x_S = \left(1 - \frac{L}{L_{max}}\right)h_S \qquad 0 \leq L \leq L_{max}$$

$$= h_S - D_S$$

The total measured deflection becomes

$$D_T = \frac{Lh_B}{YA_B} + \frac{h_S L}{L_{max}}$$

using equations (1) and (2a). Thus a linear load-deflection curve is obtained from a linear area function. In this example the slope dL/dD_T of the calculated curve is less than the Hooke's law slope.

An area function is now considered for which the area decreases with x_S as a power less than one. Such a function is

$$A_S = A_B\left[1 - \left(\frac{x_S}{h_S}\right)^2\right] \qquad 0 \le x_S \le h_S \tag{6}$$

Hence,

$$x_S = h_S\sqrt{1 - \frac{L}{L_{max}}} \qquad 0 \le L \le L_{max}$$

and

$$D_T = \frac{Lh_B}{YA_B} + h_S\left(1 - \sqrt{1 - \frac{L}{L_{max}}}\right)$$

The slope equation is

$$\frac{dL}{dD_T} = \frac{YA_B}{h_B}\left(\frac{\sqrt{1 - \frac{L}{L_{max}}}}{\sqrt{1 - \frac{L}{L_{max}}} + \frac{Yh_S}{2\sigma_Y h_B}}\right)$$

From this equation the initial portion of the load-deflection curve is linear, and its slope is less than the Hooke's law slope. As loading proceeds greater departures from Hooke's law occur, and as $L \to L_{max}$ the slope of the load-deflection curve approaches zero. The result of this type of area function (eq. (6)) is a load-deflection curve which has an artificial yield phenomena and an initial slope lower than the elastic line.

To estimate the magnitude of the initial slope of the load-deflection curve, assume $h_S = 10^{-4}$ inch (2.54 μm) and use the constants of table I. With these values the initial slope of the calculated load-deflection curve is 0.37H where $H = YA_B/h_B$ is the Hooke's law slope. Thus, a 63-percent reduction in initial slope results from this area function.

TABLE I. - CONSTANTS FOR NaCL AND STEARNS-GOTSKY EXPERIMENTS

Young's modulus, Y, psi (N/m^2)	4×10^6 (27.6×10^9)
Yield stress, σ_Y, psi (N/m^2)	160 (1.10×10^{12})
Sample cross-sectional area, A_B, sq in. (sq cm)	1/16 (0.403)
Sample height, h_B, in. (cm)	0.75 (1.91)

An area function is considered for which the area decreases with x_S at a rate faster than linear. Such a function would be

$$A_S = A_B\left(1 - \frac{x_S}{h_S}\right)^2 \qquad 0 \le x_S \le h_S \tag{7}$$

Hence,

$$x_S = h_S\left(1 - \sqrt{\frac{L}{L_{max}}}\right) \qquad 0 \le L \le L_{max}$$

and

$$D_T = \frac{Lh_B}{YA_B} + \sqrt{\frac{L}{L_{max}}}\, h_S$$

The equation for the slope of the load-deflection curve is

$$\frac{dL}{dD_T} = \frac{YA_B}{h_B}\left(\frac{\sqrt{L}}{\sqrt{L} + \frac{YA_B h_S}{2h_B\sqrt{L_{max}}}}\right)$$

From this equation it is seen that the initial slope of the load-deflection curve is zero. As the applied load increases, the slope of the calculated load-deflection curve increases. From the parameter values presented previously it follows that as $L \to L_{max}$ the slope of the calculated curve approaches a value of $0.37\,H$ where H is the slope of the Hooke's law line.

A more complex area function is obtained by joining together the two parabolic functions of equations (6) and (7), such that the area function and its slope remain continuous at the junction. Such a set of area functions are

$$A_S = A_B\left(1 - \frac{x_S^2}{h_1^2}\right) \qquad 0 \le x_S \le \frac{1}{2}h_S$$

$$A_S = 2A_B\left(1 - \frac{x_S}{h_S}\right)^2 \qquad \frac{1}{2}h_S \le x_S \le h_S$$

where $h_1 = h_S/\sqrt{2}$. The resulting equations for the "measured" deflections are

$$D_T = h_S\left(1 - \sqrt{\frac{1}{2} - \frac{L}{2L_{max}}}\right) + \frac{Lh_B}{YA_B} \qquad \frac{1}{2}L_{max} \le L \le L_{max}$$

$$D_T = h_S\sqrt{\frac{L}{2L_{max}}} + \frac{Lh_B}{YA_B} \qquad 0 \le L \le \frac{L_{max}}{2} \tag{8}$$

With the use of the constants of table I and $h_S = 2\times10^{-4}$ inch (5.08 μm), the load-deflection curve is computed for this example. The result is shown in figure 5.

In the roughness model described previously the contact area function A_S determines the shape of the resulting load-deflection curve. If the area function has a low slope for values of x_S near h_S, the load-deflection curve will display a foot. If the area function has a low slope for values of x_S near zero, a distortion will occur in the yield region of the load-deflection curve. The precise functional form of A_S will determine other details of the load-deflection curve.

Extension of the model to include more realistic sample deformation properties should not significantly alter the results. If work hardening is permitted to occur and a more realistic yield phenomena is provided, the effects of surface roughness will remain. If plastic deformation of the material is permitted in the roughness region, the contact area function will become sensitive to previous deformations. Work hardening, different yield properties, and similar refinements complicate considerably the calculation of the deflection of the roughness region; however, the non-Hookean effects should remain.

In general, the foregoing model described non-Hookean load-deflection data in terms of plastically deformed surface roughness. If the sample material has plastic deformation properties that are truly dependent on testing rates, prior deformation, etc., the model indicates non-Hookean data should display some sensitivity to these various factors. However, the converse is not necessarily true. A sensitivity of the non-Hookean data to a particular factor in no way shows that the sample material has real plastic deformation properties which are also sensitive to that factor. For example, a systematic method of sample treatment may produce systematic changes in the geometric profile of the surface roughness (i.e., the area function) and also may produce systematic differences in non-Hookean effects. In such a situation, there may be no difference in the deformation properties of the sample bulk.

EXPERIMENTAL

Specific experiments were performed to determine if surface roughness does exist on prepared NaCl surfaces. These experiments were optical and electron-microscopic surface examinations; they show that there is enough surface roughness to produce the non-Hookean effects reported in references 1 to 4.

Load-deflection experiments were also performed to determine the effect of surface roughness on the load-deflection data obtained in the manner of reference 3. In these experiments two simultaneous deflection measurements were made; one combining sample bulk and surface deflection (using the method of ref. 3), the other measuring only deflection of the sample bulk. Only the former deflection measurement shows non-Hookean results of the Stearns-Gotsky type.

Microscopic Examination of Surfaces

Several types of prepared surfaces were examined with an optical interference microscope. The photomicrographs show that the roughness present on surfaces prepared by the methods of reference 3 cannot be specified reliably by interference methods. The scope of this problem is revealed by photomicrographs of different surfaces, ranging from a mirror-polished metal surface to a NaCl surface prepared in the manner of reference 3.

Figure 6 is an interference photomicrograph of a highly polished metal surface. Note the high specular reflection, as shown by the contrast between light and dark fringes, uniformity of fringe spacing, and linearity of fringes across the entire field of view. Some highly localized defects are seen. These defects are most important from the standpoint of compression experiments of the Stearns-Gotsky type, since they produce a contact area which changes with deflection.

A photomicrograph of a cleaved NaCl surface is shown in figure 7. Plateaus of varying elevation are observed together with large scratches or cleavage marks. The interference microscope can be used to good advantage on such a surface since it can measure elevation differences by measuring fringe displacement. The depths of scratches can be determined in a similar manner. One plateau is seen to be about 10 microinches (0.25 μm) above its neighbor since the fringes are displaced one full fringe width. It would be hard to specify an rms surface finish for such a surface without knowing the size and distribution of plateaus over the whole surface. This surface should produce large non-Hookean effects in a Stearns-Gotsky type experiment. The deflection effects of such surfaces would be present in the data reported in reference 1.

Figure 8 is an interface photomicrograph of a cleaved NaCl crystal polished on

4/0 emery polishing paper, showing destruction of specular reflection over some areas and extreme irregularity over others. Surface irregularities 40 and 50 microinches (1.0 to 1.3 μm) high are present in large numbers. A determination of peak-to-peak or rms surface roughness in this case is virtually impossible.

The ground surface shown in figure 8 was water polished in a 1:4 solution of H_2O:HCl. About 5×10^{-3} centimeter of surface was removed. The interference micrograph shown in figure 9 shows that specular reflection is restored; however, large scale variations in surface elevation are present.

Figure 10 shows a surface of NaCl polished with 0.05×10^{-4} centimeter silica particles on a lubricated cloth backing. The fringe pattern is again specular, and fringes are somewhat straight and parallel. Surface irregularities of about 5 microinches (0.13 μm) (1/2 a fringe width) are common together with many large scratches.

A surface prepared by the Stearns-Gotsky method is shown in figure 11. The final lapping for this surface is performed with dry 4/0 emery paper. This paper has a grit size 300 times larger than the grit used in the final lapping of the surface shown in figure 10. The photomicrograph shows that the Stearns-Gotsky preparation destroys specular reflection.

The loss of specular reflectivity suggests that the surface is composed of small grain roughness as opposed to flat regions with differing elevations. Small grain roughness refers to a surface composed of chunks or lumps of material with a mean diameter or dimension about equal to or less than the illumination wavelength ($\sim21\times10^{-6}$ in., 0.53 μm). A small grain roughness was detected with an electron microscope.

The electron microscope was used to study the small grain surface structure of prepared NaCl samples. Micrographs were made from replicas of the particular surface. The shadow angle is 45°, and shadows appear as white regions in the reproductions.

Figure 12 is a photomicrograph of a cleaved NaCl surface. The resolution of this figure is about 40 times greater than in figure 7. The plateau structure is evident in both figures. The electron micrograph shows a 50-microinch (1.27 μm) step between plateaus. Aside from some scattered debris and small craters, the surface of a plateau is relatively smooth and should produce specular reflection like that seen with the optical microscope (fig. 7).

A NaCl surface prepared in the manner of Stearns and Gotsky was examined with the electron microscope; figure 13 is a representative photomicrograph. The increased resolution of this technique reveals the small grain roughness which destroys the specular reflection of the surface (see figs. 8 and 11). The surface roughness is composed of lumps with a somewhat uniform distribution in size. From this photomicrograph one can resolve surface lumps from a few microinches (0.01 μm) to some 50 microinches (1.3 μm) in size. It is impossible to assign a roughness value to such a surface with any precision; however, the reported value of 4 microinches (0.1 μm) rms (ref. 3) is certainly erroneous.

Load-Deflection Experiments

Compression load-deflection experiments were performed on single crystal NaCl, KBr, KCl, and LiF. These experiments involved two simultaneous deflection measurements. The first deflection measurement technique is that of Stearns and Gotsky (see fig. 2 and ref. 3). The second deflection measurement employed a triple-plate capacitance gauge (see fig. 14). Because of its unique character and its importance in the experimental data to be presented, a somewhat detailed description of the capacitance gauge is given in appendix A.

Load-deflection experiments were performed on single crystals of NaCl, LiF, KBr, and KCl. Most test samples were rectangular prisms with ⟨100⟩ loading faces. Rectangular prism dimensions were nominally 0.25 by 0.25 by 0.75 inch (0.635 by 0.635 by 1.91 cm). One NaCl sample with ⟨111⟩ end faces was also tested. This sample was a right circular cylinder 0.25 inch (0.635 cm) in diameter and 0.75 inch (1.91 cm) high. The compression axis was within 6° of the ⟨111⟩ direction.

All ⟨100⟩ loading surfaces were polished as described in reference 3, with final lapping on dry 4/0 emery polishing paper. The ⟨111⟩ NaCl sample was tested without polishing the loading surfaces. The final preparation step was cementing the capacitance gauge onto the sample as described in appendix A.

The sample to be tested was mounted in the compression apparatus shown in figure 2. The metal beam extension was replaced with a Lucite extension to prevent interaction with the electric field of the capacitance gauge. The loading anvil and probe were electrically grounded to avoid perturbation of the capacitance gauge.

The drive rod of the compression apparatus was loaded by the testing machine crosshead through a rubber cylinder. This aids in isolating the sample from vibrations in the moving crosshead. The energy stored in the rubber cylinder obscures yield-point phenomena (ref. 5) if any exists, and results in additional sample strain immediately after the start of the unloading portion of a compression cycle.

The recording of the load-deflection data produced by the Stearns and Gotsky method was performed as described in reference 3. The recording of the load-deflection data obtained with the capacitance gauge used the electronic circuitry shown in figure 15.

Figure 16 shows the load-deflection data obtained for polished ⟨100⟩ NaCl. The load and deflection scales are shown. The Hooke's law slope is shown as a line in figure 16(b) and as a shaded region in figure 16(a). The shaded region results from uncertainties in the active gage length of the capacitance gauge. This uncertainty is a consequence of attaching the gauge with cement. It is seen by comparing the data presented in figures 16(a) and (b) that the deflection measurement method of Stearns and Gotsky shows an apparent deformation that is not displayed in the capacitance gauge measurement.

The load-deflection curves for potassium bromide (KBr), potassium chloride (KCl),

and lithium fluoride (LiF) are shown in figures 17(a) and (b), 18(a) and (b), and 19(a) and (b), respectively. In each case, a foot is seen in the data obtained by the Stearns-Gotsky method, whereas the capacitance gauge data show no unusual initial deformation. In figures 17 to 19 a section of data has been deleted in the plastic region. The magnitude of the omitted deflection is indicated. The purpose of this deletion was to permit presentation of the unloading portion of the measured data.

The load-deflection data for unpolished ⟨111⟩ NaCl is shown in figure 20. A large foot region is observed in the data obtained by the Stearns-Gotsky method, whereas no upward curvature is observed in the capacitance gauge data. A significant increase in work-hardening rate is observed with the ⟨111⟩ orientation.

Reference 3 places considerable emphasis on the complete loading-unloading cycle and the hysteresis loops obtained after several cycles. The implication is that a nonlinear unloading curve confirms the significance of the nonlinear loading curve. Figure 21 gives a comparison of cyclic load-unloading data. Once again the Stearns-Gotsky method of measurement produces non-Hookean data for each cycle whereas the capacitance gauge data is relatively linear.

All the load-deflection data obtained in this investigation are consistent in that (a) non-Hookean effects are always observed with the deflection measurement method of Stearns and Gotsky and (b) load-deflection data obtained with the capacitance gauge always displays Hookean response.

Discussion

The experimental data of references 1 to 4 were obtained in compression, four-point bending, and creep tests. While much of the preceding comment is directed specifically to the compression experiment, each of these other tests suffers from the same error in experimental technique. The bending data in addition to surface roughness problems also include deflections arising from the indentation of the sample by the loading edges. Thus, all deflection measurements reported in these references must be viewed with caution.

Other aspects of the experimental data deserve comment. For example, there is the question of whether a surface roughness analysis can account for the pretreatment, testing rate, size effects, and vibration effects reported in these references.

It is possible for a given pretreatment to produce a significant change in foot length, by a systematic alteration of the surface roughness. Some pretreatments by their very nature suggest large changes in surface condition. Grinding and water polishing should alter an as-cleaved surface considerably. The magnitude of these changes can be estimated from the photomicrographs presented earlier.

In addition to surface roughness, it must be realized that some pretreatments alter the mechanical properties of the sample. The foot length defined in reference 1 is sensitive to both surface roughness and yield stress. For pretreatments which alter the mechanical properties of the sample, it is impossible to separate surface and bulk effects with foot length data alone. Pretreatments such as quenching and X-irradiation combine surface and bulk changes. Hibi et al. (ref. 6) have shown by electron microscopy that alkali halide single crystals develop surface roughness from X-irradiation. The quenching treatment of reference 1 gives a large-scale curvature to the loading faces, presumably because of the large thermal strains. Both treatments alter the yield stress of the sample; it is hard to say whether surface or bulk effects play the dominant role in altering the foot length.

The effect of testing rates on the non-Hookean effect reported in reference 3 means that the observed deflection was found to be time dependent. It is not surprising to find time-dependent plastic flow in the highly deformed surface roughness region. Such effects would be small, and there is doubt that this experimental technique can resolve these effects reliably.

The size effect of reference 3 consists of a comparison of load-deflection data for samples of different heights. The data are displayed in a stress-strain plot. The direction of the size effect is that samples of smaller height have a larger non-Hookean effect in the stress-strain comparison. A surface roughness analysis would also predict a size effect in which the size of the non-Hookean effect varies inversely with bulk sample height.

A dynamic shaking experiment, described in reference 3, purports to show a regeneration of the non-Hookean effect by audio frequency vibration. The authors interpret the results as arising from the internal stress relaxation of the sample. The results can also be explained in terms of changes in surface roughness that result from bouncing the sample on the shaker table.

CONCLUDING REMARKS

The data reported in references 1 to 4 contain a large experimental error which arises from the inclusion of surface roughness deflections with sample deflections. This error produces the low initial slope of the stress-strain curve and may also alter the yield effects. All the data presented in these references are subject to this error.

An analysis of this experimental error predicts the size and form of the non-Hookean effect in terms of a simple surface roughness model. The model seems sufficiently complete to explain the qualitative observations of pretreatment, testing rate, size, and

shaking effects as reported in references 1 to 3. Experimental evidence shows that the non-Hookean effect arises from the loading surface region of the sample. These findings indicate that the origin of the non-Hookean effect is the roughness of the loading surfaces.

Lewis Research Center,
National Aeronautics and Space Administration,
Cleveland, Ohio, November 9, 1967,
129-03-15-03-22.

APPENDIX A

CAPACITANCE GAUGE

The need for a simultaneous and independent deflection measurement resulted in the design of a triple-plate capacitance gauge which is described here. This device is easily adaptable to the Stearns-Gotsky apparatus; has better linearity, sensitivity, and overall accuracy; and can measure deflections over an arbitrarily large gauge length. In the form described here it is not suitable for use with metal samples.

The capacitance gauge (fig. 14) was fashioned from three circular aluminum plates, three bakelite spacer posts, and a molded fiber glass - epoxy tube. The top and bottom plates were supported near the base of the sample; the gauge plate was supported near the top of the sample. The top and bottom plates were separated 0.440 inch (1.12 cm) by the bakelite spacers.

The topmost end of the fiber glass - epoxy tube had a square or circular fillet of epoxy to adapt to rectangular or cylindrical geometry. Cemented to the bottom plate was a sample adaptor plate. This plate was a circular aluminum disk with either a square or circular hole through its center to facilitate attachment to the two specimen geometries.

The capacitance gauge was attached to the sample with an acrylic base cement. To assist in mounting the sample in the capacitance gauge, four bakelite spacer blocks held the gauge plate centered and rigid with respect to the top and bottom plates. The sample adaptor plate and the epoxy fillet of the fiber glass - epoxy tube were cemented to the sides of the sample, so that the capacitance gauge would measure the sample deflection over a sample gauge length nearly three quarters of the total sample height.

Figure 15 shows the associated circuitry. An oscillator with low harmonic content drives the primary winding of a transformer and the reference channel of a phase sensitive detector. The transformer secondary winding is connected to the top and bottom plates of the capacitance gauge. In parallel with the secondary winding is an electrical zero and phase shifting network composed of R_1, R_2, C_1, and C_2. The function of this network is to produce a voltage null at the input of amplifier A. Amplifier A is a low-noise, high-gain, ac amplifier with selectable pass band. The output of amplifier A is applied to the signal channel of the phase-sensitive detector, which produces a dc output voltage proportional to that portion of the signal voltage produced by the capacitance gauge which bears the proper phase relation to the reference channel voltage.

Analysis of the circuit of figure 15 is useful in determining the properties of the capacitance gauge. For this purpose the electrical zero and phase-balance network will be ignored. The circuit to be analyzed is shown in figure 22.

Ignoring end effects of capacitors C_{11} and C_{21} (see fig. 22) and assuming $\delta/D \ll 1$ yield the voltage V_R:

$$\left.\begin{aligned} V_R &= \frac{2E\delta}{D}\left[\frac{1}{\frac{\beta}{Z}D + 2}\right] \\ Z &= \frac{1}{\frac{1}{R} + i\omega C_3} \end{aligned}\right\} \tag{9}$$

where $2E$ is the voltage applied to the top and bottom plates of the gauge, δ is the displacement of the gauge plate (in in.), $2D$ is the separation of the top and bottom plates of the gauge (in in.), $\beta = -i/KA\omega$, ω is the angular frequency, K the dielectric constant of air, and A the area of a capacitor plate.

Equation (9) shows the voltage V_R to be directly proportional to gauge plate displacement δ and to applied voltage $2E$. Consequently, the triple-plate capacitange gauge is a linear device with easily variable sensitivity. To estimate the sensitivity obtainable, let A = 3 square inches (19.4 cm^2), $K = 0.0885\times10^{-12}$, $\delta = 10^{-6}$ inch (0.025 μm) E = 50 volts, D = 1 inch (2.54 cm), $R = 10^7$ ohms, $\omega = 10^6$ sec^{-1}, and $C_3 \approx 10^{11}$ farads. Under these conditions the sensitivity S is

$$S = \frac{2.5 \text{ microvolts}}{\text{microinch displacement}} = \left(\frac{100\ \mu V}{\mu m}\right)$$

Sensitivities of this magnitude are adequate for the purpose of this investigation.

Linearity of the capacitance gauge was measured by mounting the gauge on a micrometer driven calibration jig. Total system calibration was also performed. Measured linearity was within 4.5 percent over a deflection range of 6×10^{-3} inch (152.0 μm) from the null position. Since the micrometer used in the calibration has a resolution of 5×10^{-5} inches (1.27 μm) a 5-percent error in positional measurement occurs for a 10^{-3} inch (25.4 μm) displacement. Examination of the linearity measurements reveals that the principal source of error arises from positional errors of the micrometer. At large displacements from null ($\sim 150\times10^{-3}$ in. (3800 μm)) nonlinearities were observed. All experiments to be reported utilize a gauge plate displacement of less than 10^{-3} inch (25.4 μm) from the null position.

A potential source of calibration error can arise from the improper setting of the phase-sensitive detector system. The reference voltage obtained from the oscillator (see fig. 15) is shifted in phase and used to actuate the demodulators in the phase-

sensitive detector. In principle, the gauge plate should be displaced from null and the phase shift of the reference voltage adjusted to produce a maximum direct-current output voltage. In these experiments the capacitance gauge was cemented to the sample so that displacement from null could only be achieved by deforming the sample. Consequently, the phase-shifting network of the phase-sensitive detector was approximately set and the first load-deflection cycle was executed. The residual strain resulting from the first cycle was used to accurately adjust the phase-shifting network. Knowledge of the correct phase angle and the phase angle used during the first load-deflection cycle allows one to determine the calibration of the first cycle.

Several problems exist with the use of the capacitance gauge. The most important being thermal expansion of the sample. With ionic single crystals of the size employed here, 30×10^{-6} inch (0.76 μm) of apparent sample deflection occur for each degree centigrade of sample temperature change. Thermal drift arose mostly from air currents and was reduced significantly when the entire compression apparatus was enclosed in a plastic bag. As a consequence, thermal drift due to all sources was reduced to $\pm3\times10^{-6}$ inch (0.076 μm) during the time interval necessary to perform an experiment.

Another problem arises from the motion of metallic objects in the vicinity of the gauge itself - in particular, the motion of the drive rod before the start of the test. The magnitude of the effect is proportional to the displacement of the metal object. Prior to the start of loading the drive rod is moving with the velocity of the testing machine crosshead (~0.2 in./min (0.51 cm/min)). Upon contact of the loading anvil, rod velocity is greatly reduced so that during the entire experiment the drive rod moves only a few hundred microinches (0.2 to 0.4 μm). The effects of drive rod motion during the loading-unloading cycle are considerably smaller in magnitude than the thermal-drift effects. Estimates of this effect indicate an apparent sample deflection of less than 10^{-6} inch (0.025 μm) during the entire test.

APPENDIX B

SYMBOLS

A	area of capacitance gauge plates
A_B	sample cross-sectional area
A_S	cross-sectional area of roughness region
C_3	input capacitance of signal amplifier and cable
C_{11}, C_{21}	capacitances formed by gauge
D	spacing of top and bottom plates of capacitance gauge
D_B	deflection of sample bulk
D_S	deflection of surface roughness
D_T	total deflection
$2E$	voltage applied to top and bottom plates
H	slope of Hooke's law line
h_B	sample height
h_S	height of surface roughness
h_1	constant matching parameter
L	applied load
L_{max}	maximum load bearing capacity of sample
dL/dX	slope of load-deflection curve
P.S.D.	phase-sensitive detector
R	input resistance of signal amplifier
R_1, R_2 C_1, C_2	balance network parameter values
S	sensitivity factor
V_R	output voltage of capacitance gauge
x_P	positional coordinate of loading plate
x_S	directed distance upward above top surface of sample
Y	Young's modulus

Z impedance of input circuit of signal alternating-current amplifier

β constant, $-i/KA$

δ displacement of gauge plate

σ stress

σ_Y yield stress

ω angular frequency

REFERENCES

1. Stearns, Carl A.; Pack, Anne E.; and Lad, Robert A.: Ductile Ceramics. I- Factors Affecting the Plasticity of Sodium Chloride, Lithium Fluoride, and Magnesium Oxide Single Crystals. NASA TN D-75, 1959.

2. Stearns, C. A.; Pack, A. E.; and Lad, R. A.: Factors Affecting the Ductility and Strength of NaCl Single Crystals Tested in Flexure. J. Appl. Phys., vol. 31, no. 2, Feb. 1960, pp. 231-234.

3. Stearns, Carl A.; and Gotsky, Edward R.: Non-Hookean, Premacroyield Stress-Strain Behavior of Several Ionic Single Crystals. NASA TN D-2545, 1964.

4. May, Charles E.; Grimes, Hubert H.; and Lad, Robert A.: Ductile Ceramics. II- Introductory Study of Ductility in Polycrystalline Sodium Chloride and Magnesium Oxide. NASA TN D-76, 1959.

5. Johnston, W. G.: Yield Points and Delay Times in Single Crystals. J. Appl. Phys., vol. 33, no. 9, Sept. 1962, pp. 2716-2730.

6. Hibi, Tadatosi; and Ishikawa, Kazuo: Electronmicroscopic Observation of Coloured and Bleached Alkali-Halide Crystals. J. Phys. Soc. Japan, vol. 13, no. 7, July 1958, pp. 709-716.

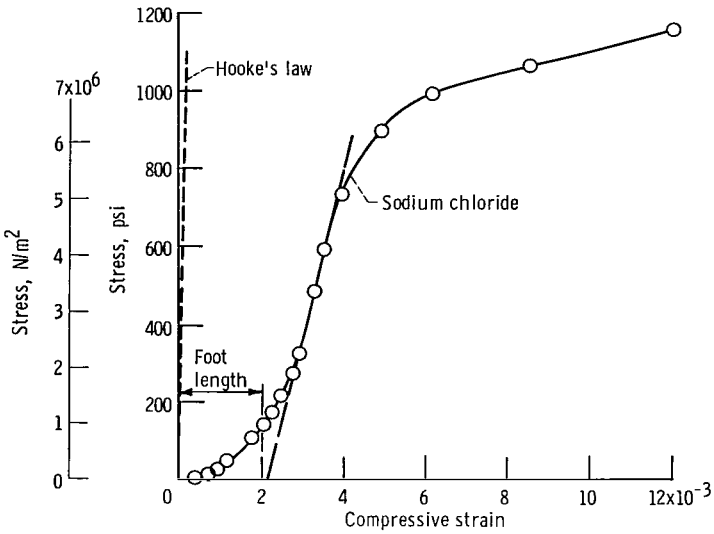

Figure 1. - Initial portion of stress-strain curve for sodium chloride single crystal tested in compression as reported in reference 1. Foot length as defined in reference 1 is 1.6×10^{-3} inch (4.06×10^{-3} cm). Sample length, 0.750 inch (1.91 cm).

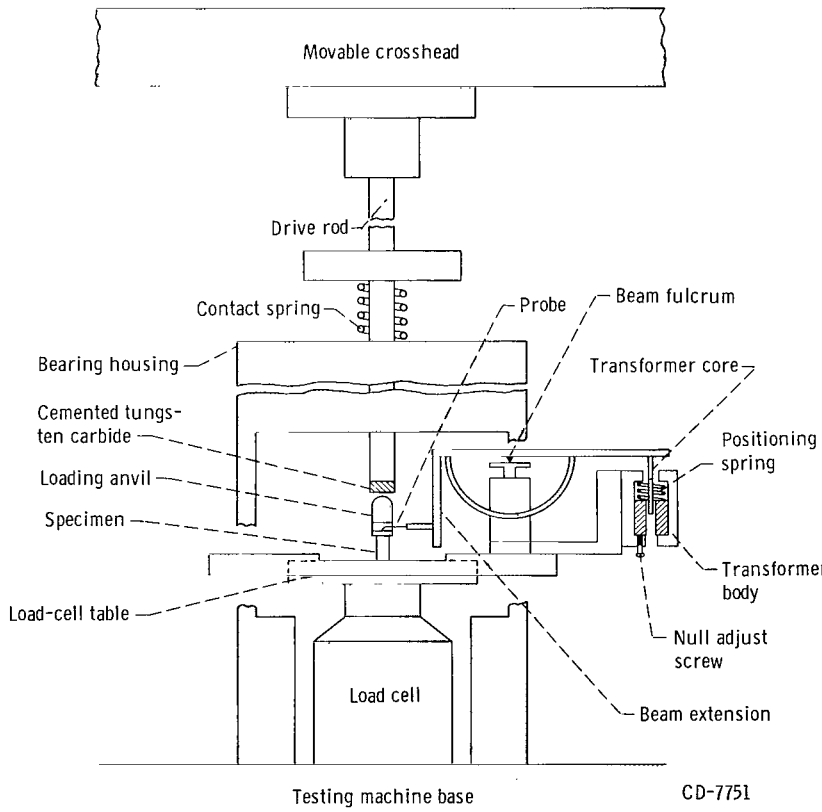

Figure 2. - Schematic drawing of Stearns-Gotsky compression apparatus (ref. 3).

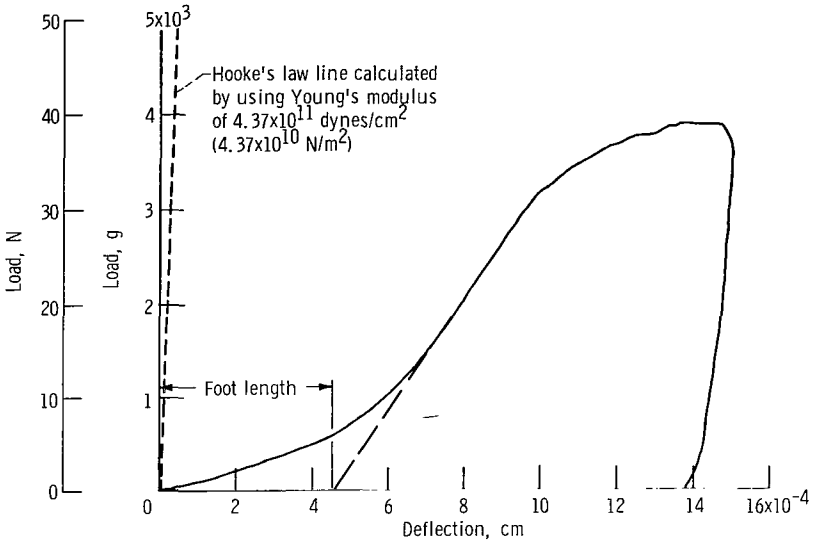

Figure 3. - Initial portion of load-deflection curve for sodium chloride single crystal tested in compression (reported in ref. 3). Foot length as defined in reference 1 is 1.77×10^{-4} inch (4.5×10^{-4} cm).

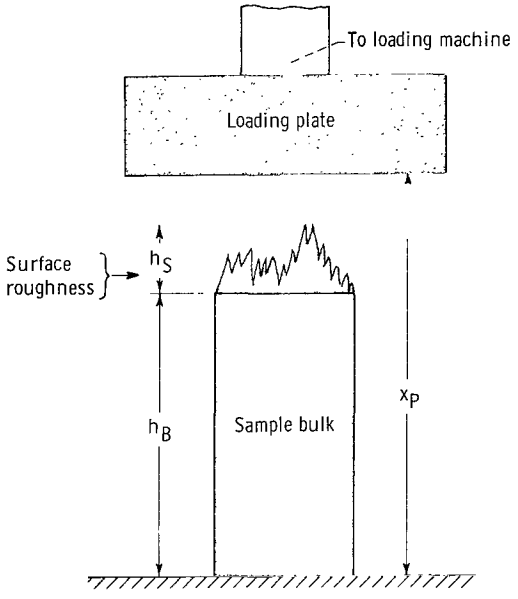

Figure 4. - Schematic diagram of the analyzed compression experiment. Surface roughness of the sample loading surfaces is shown. No applied load.

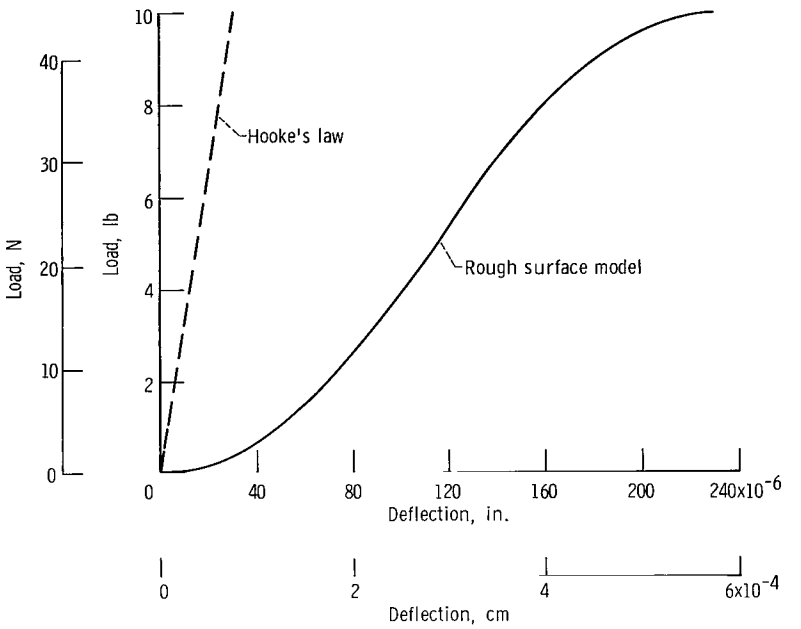

Figure 5. - Load-deflection curves calculated from equation (8).

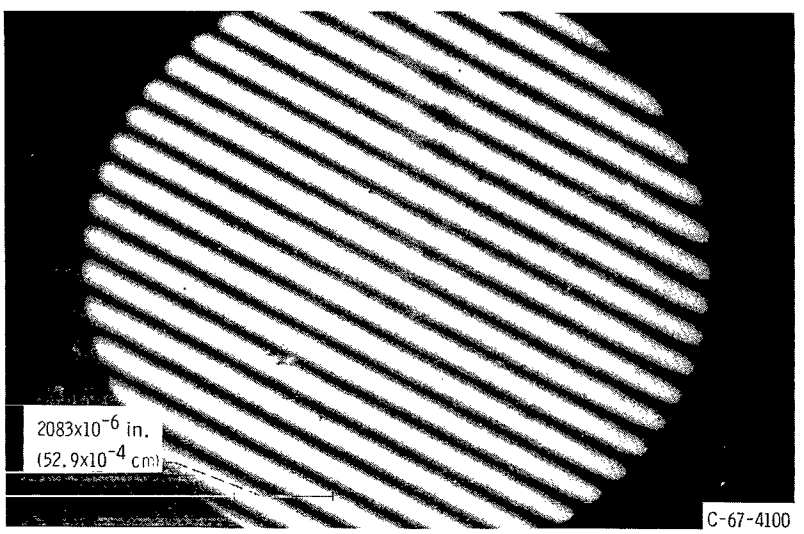

Figure 6. - Optical interference micrograph of a highly polished metal surface. Clarity of the fringes attest to the high specular reflectivity of this surface.

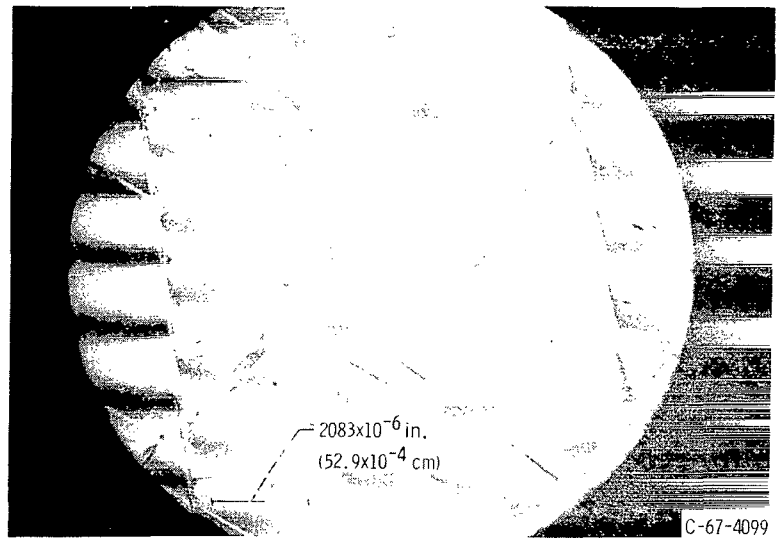

Figure 7. - Optical interference micrograph of an as-cleaved sodium chloride surface. Plateaus of specular reflectivity exist at varing elevations. Fringe displacement can be used to determine elevation differences.

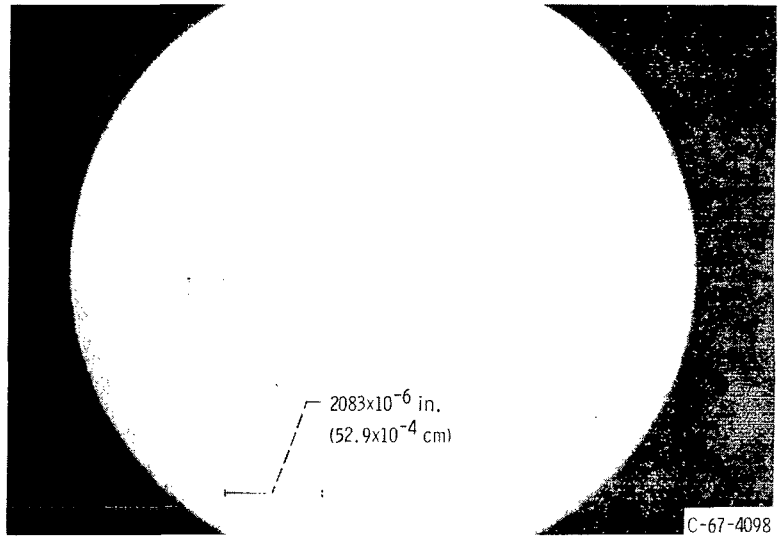

Figure 8. - Optical interference micrograph of an as-cleaved sodium chloride polished on 4/0 metalographic emery polishing paper. The large displacements of the fringes attest to the severe roughness of this surface. Some areas are present wherein the roughness is so severe that no fringe pattern is resolvable by the microscope.

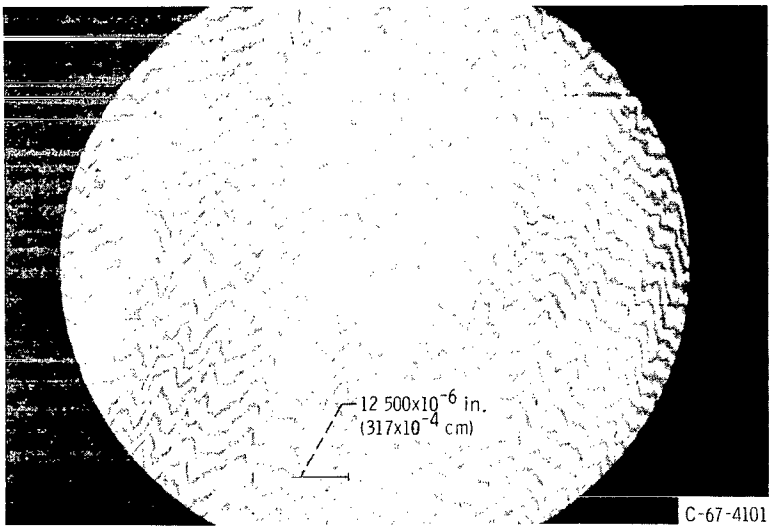

Figure 9. - Optical interference micrograph of the surface shown in figure 8 after it has been water polished in a $HCl-H_2O$ solution. Specular reflection is present while extreme irregularity remains.

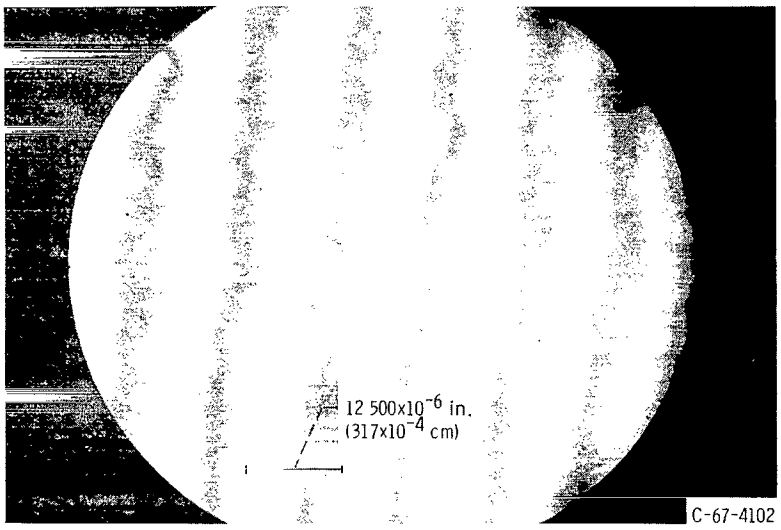

Figure 10. - Optical interference micrograph of a sodium chloride surface polished with 0.05-micron silica dust on a lubricated silk felt backing. While many deep scratches are visible, specular fringes are present.

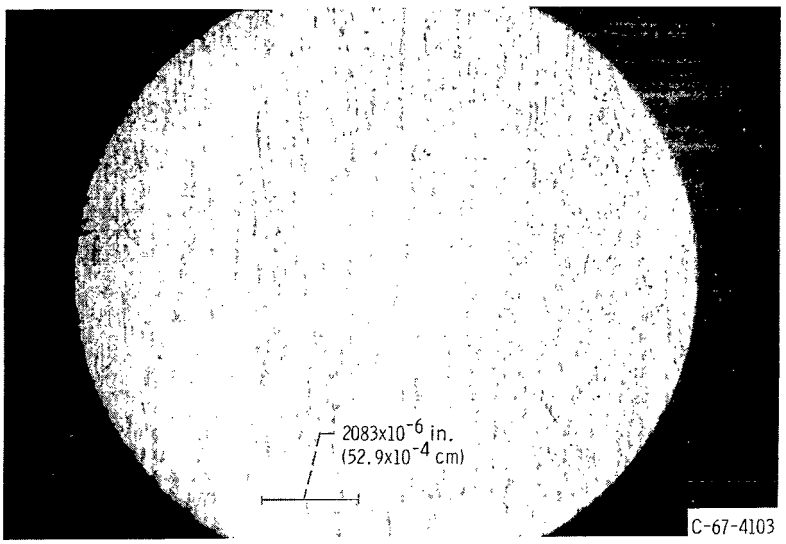

Figure 11. - Optical interference micrograph of a sodium chloride surface prepared by the Stearns-Gotsky method. Specular reflection is absent which suggests a small grain roughness. Final lapping for this surface uses a grit which is 300 times larger than the grit size used in figure 10.

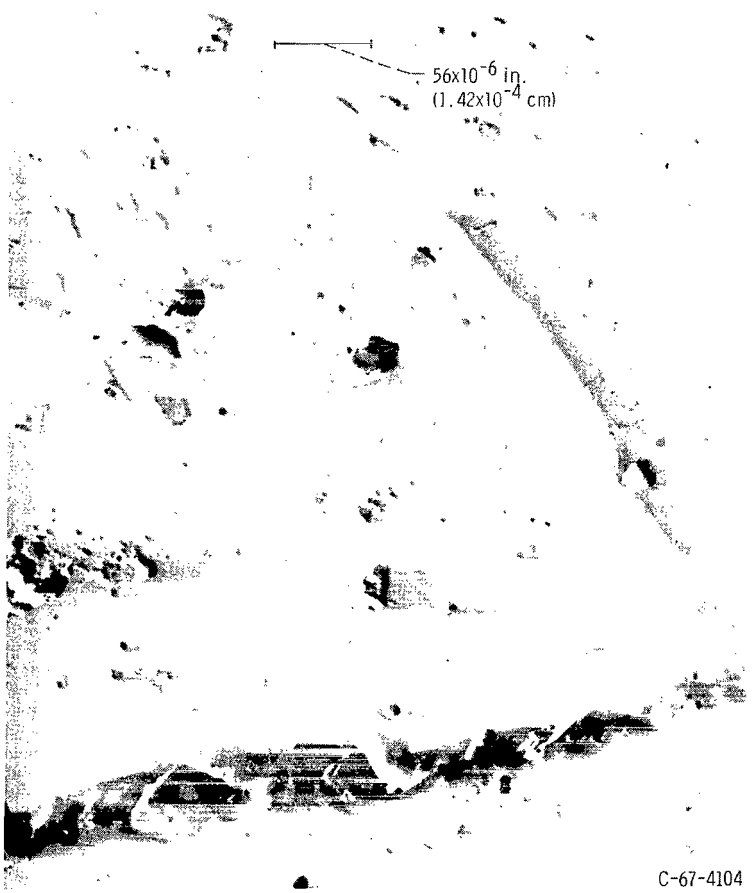

Figure 12. - Electron micrograph of as-cleaved NaCl surface. Shadow angle, 45°; total area shown, 0.232x10^{-6} square inch (1.496x10^{-6} cm^2). (Shadow areas appear light.)

Figure 13. - Electron micrograph of a polished NaCl surface. Surface was polished with 4/0 emery polishing paper by the Stearns-Gotsky method (ref. 3). Shadow angle, 45°; total area shown, 0.232x10^{-6} square inch (1.496x10^{-6} cm^2). Shadow areas appear light.)

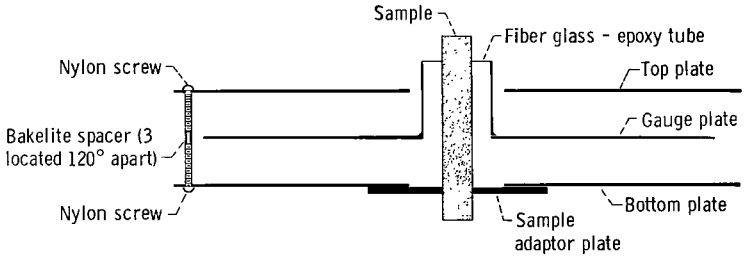

Figure 14. - Schematic diagram of capacitance gauge.

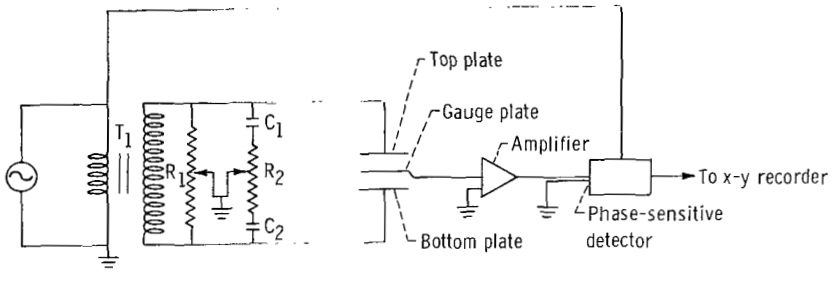

Figure 15. - Electronic circuitry employed with capacitance gauge. Amplifier A is high-gain - low-noise type with 10^7 ohm input impedance (at 100 cps).

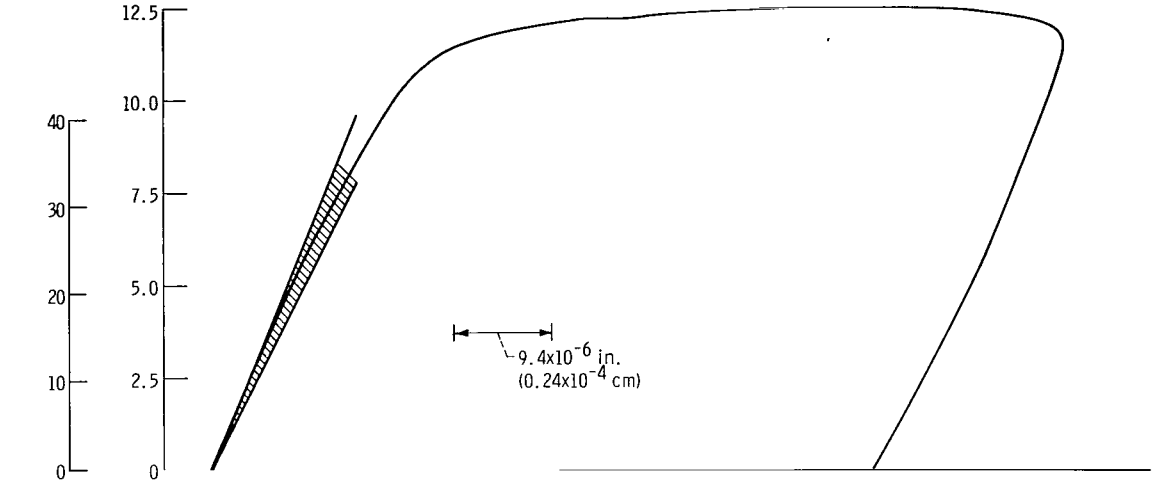

(a) Measured by capacitance gauge. Hooke's law line lies within the shaded region.

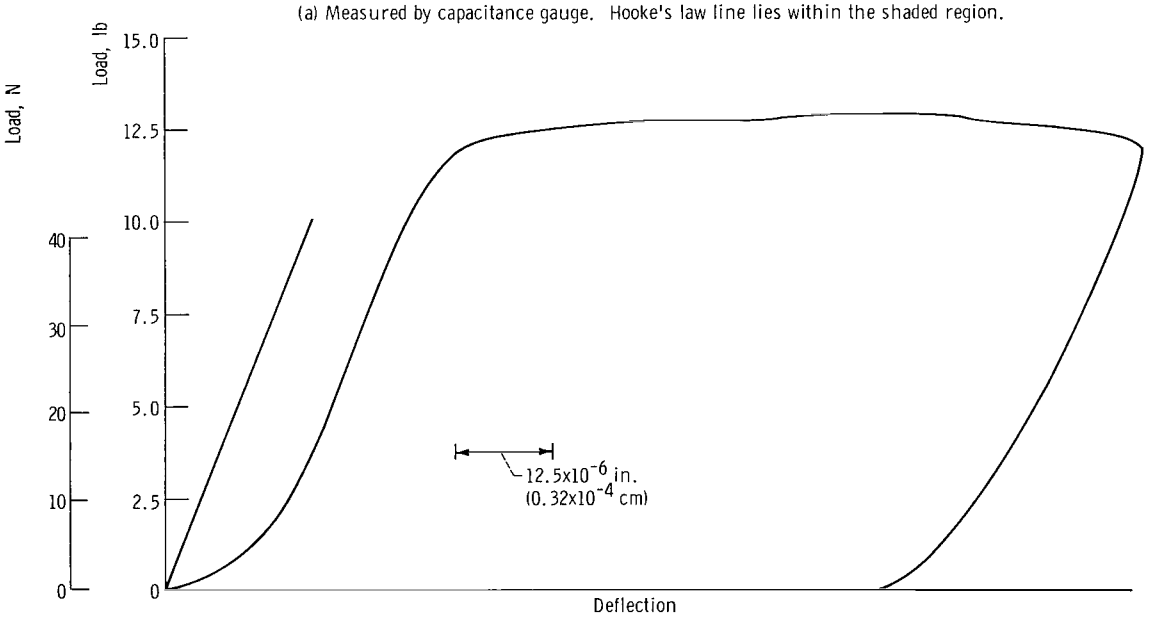

(b) Measured by Stearns-Gotsky method.

Figure 16. - Load-deflection curve for <100> sodium chloride single crystal.

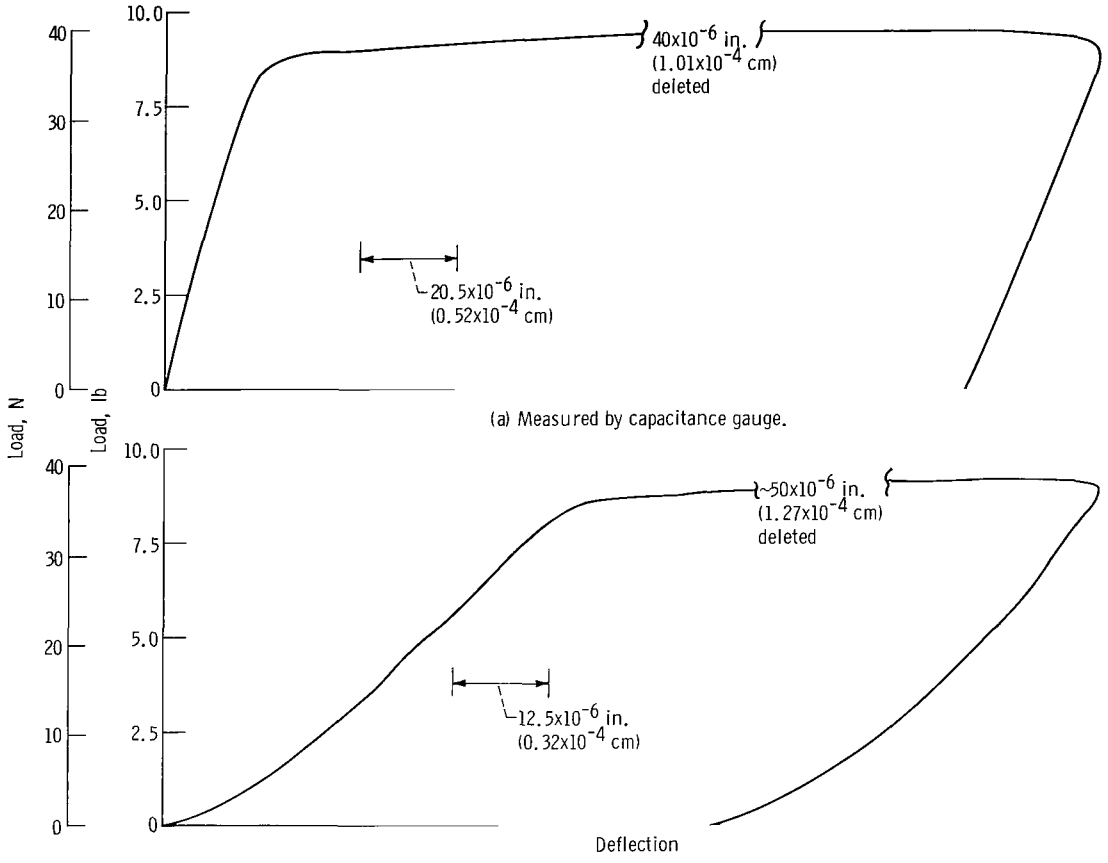

(a) Measured by capacitance gauge.

(b) Measured by Stearns-Gotsky method.

Figure 17. - Load-deflection data for potassium bromide.

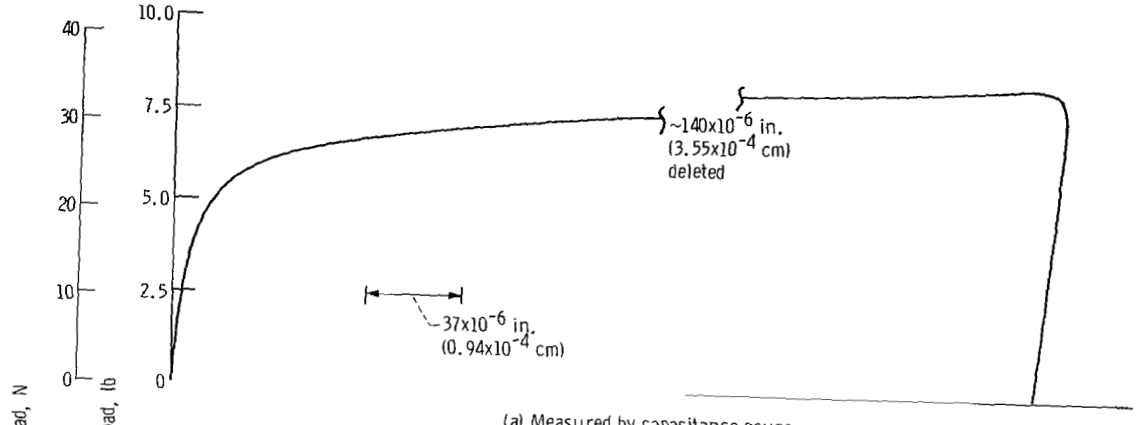

(a) Measured by capacitance gauge.

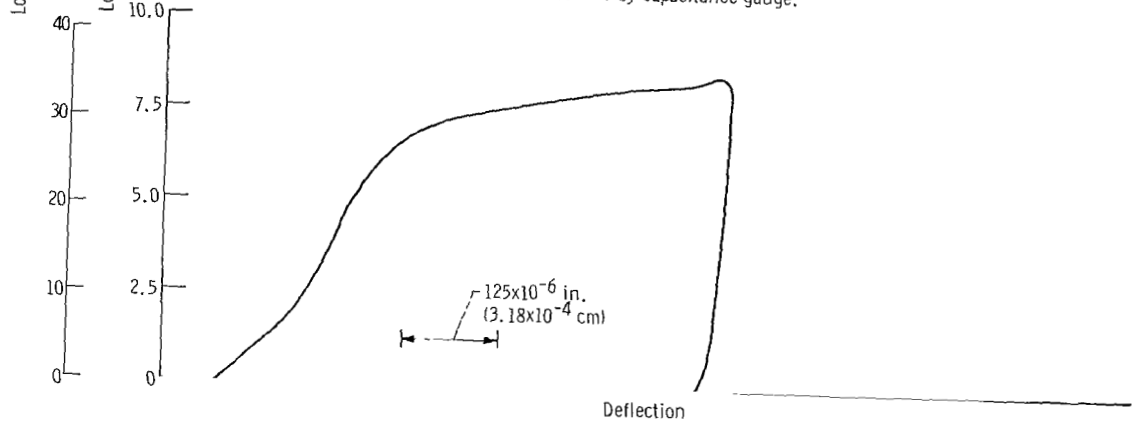

(b) Measured by Stearns-Gotsky method.

Figure 18. - Load-deflection data for potassium chloride.

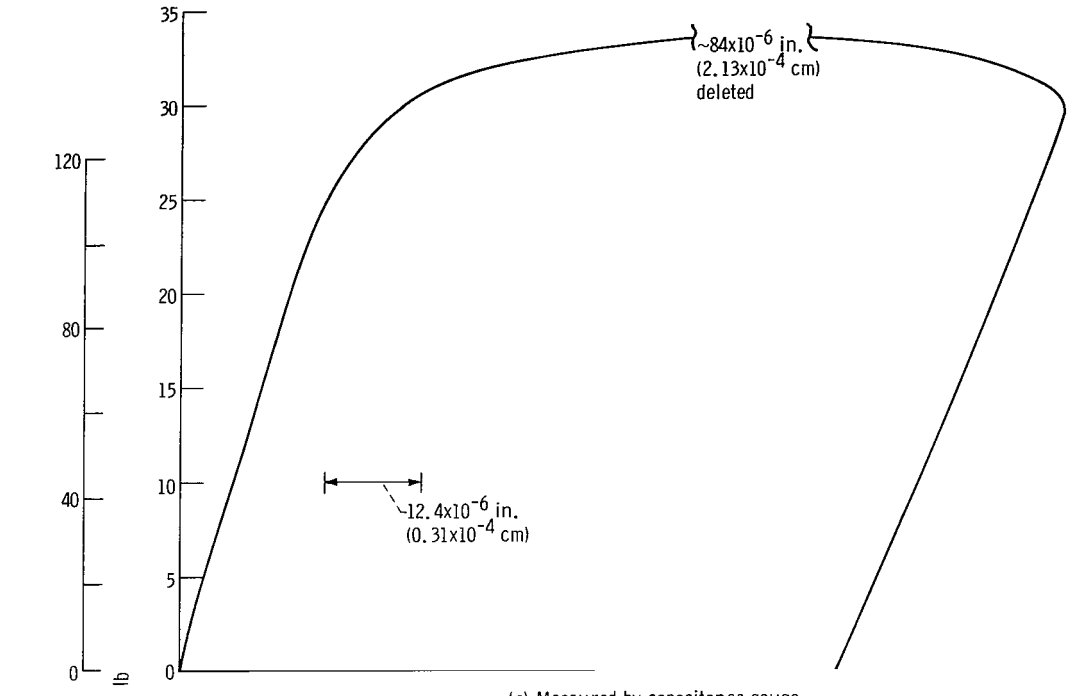

(a) Measured by capacitance gauge.

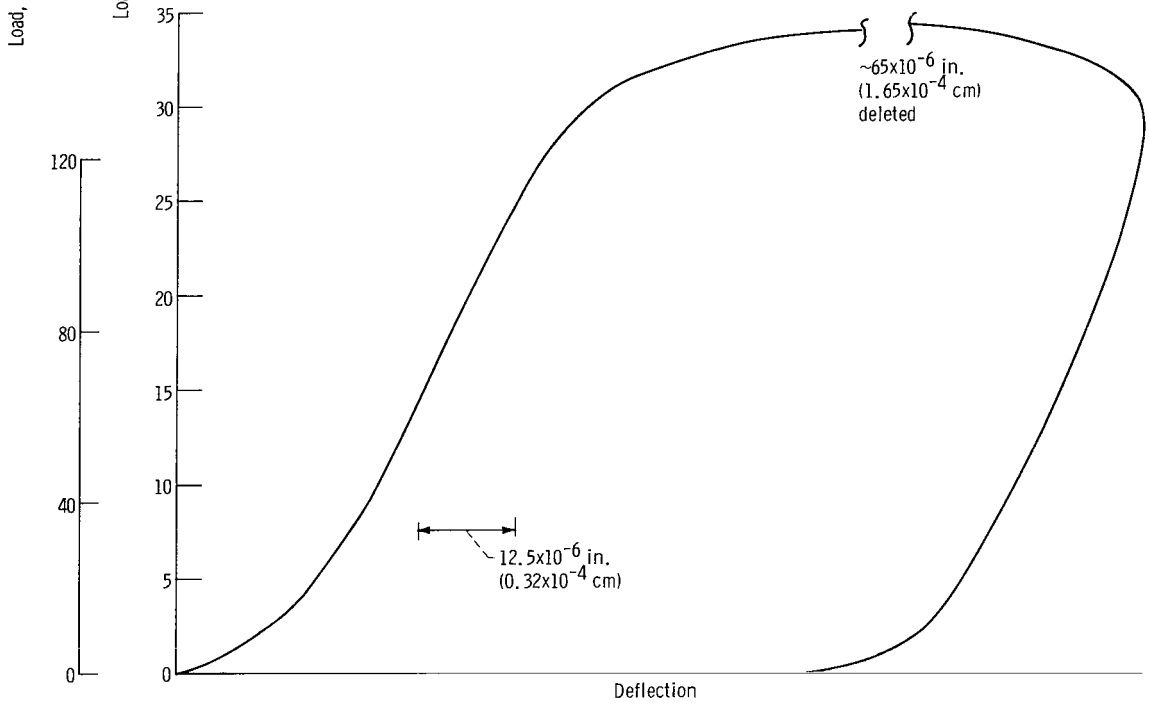

(b) Measured by Stearns-Gotsky method.

Figure 19. - Load-deflection data for lithium fluoride.

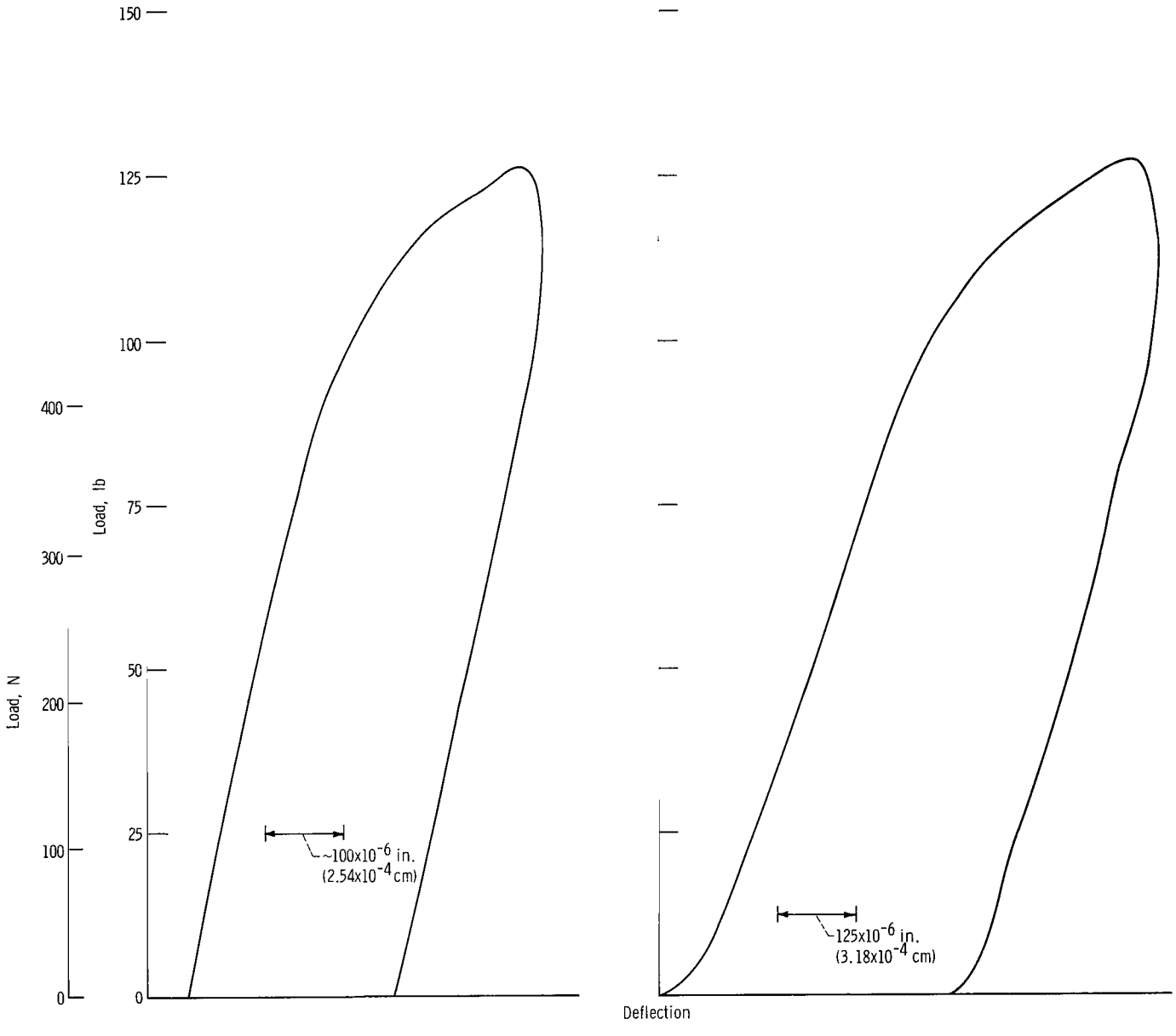

(a) Measured by capacitance gauge.

(b) Measured by Stearns-Gotsky method.

Figure 20. - Load-deflection data for sodium chloride (<111> orientation).

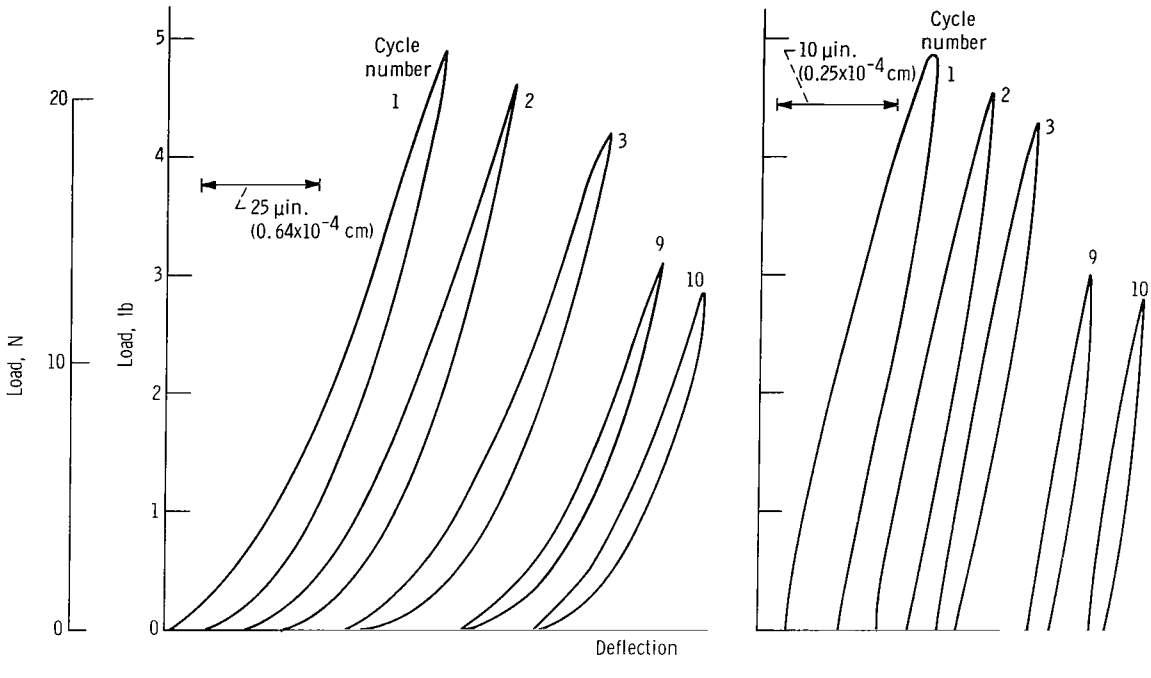

(a) Stearns-Gotsky method.

(b) Capacitance gauge method.

Figure 21. - Comparison of cyclic loading-unloading data.

C_{11} Capacitance between top plate and gauge plate
C_{21} Capacitance between bottom plate and gauge plate
C_3 Cable and amplifier input capacitance
R Amplifier input resistance
2E Voltage applied to capacitance gauge

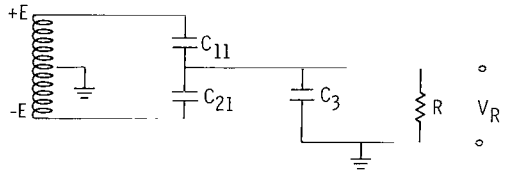

Figure 22. - Circuit used to analyze capacitance gauge.

"The aeronautical and space activities of the United States shall be conducted so as to contribute . . . to the expansion of human knowledge of phenomena in the atmosphere and space. The Administration shall provide for the widest practicable and appropriate dissemination of information concerning its activities and the results thereof."

— NATIONAL AERONAUTICS AND SPACE ACT OF 1958

NASA SCIENTIFIC AND TECHNICAL PUBLICATIONS

TECHNICAL REPORTS: Scientific and technical information considered important, complete, and a lasting contribution to existing knowledge.

TECHNICAL NOTES: Information less broad in scope but nevertheless of importance as a contribution to existing knowledge.

TECHNICAL MEMORANDUMS: Information receiving limited distribution because of preliminary data, security classification, or other reasons.

CONTRACTOR REPORTS: Scientific and technical information generated under a NASA contract or grant and considered an important contribution to existing knowledge.

TECHNICAL TRANSLATIONS: Information published in a foreign language considered to merit NASA distribution in English.

SPECIAL PUBLICATIONS: Information derived from or of value to NASA activities. Publications include conference proceedings, monographs, data compilations, handbooks, sourcebooks, and special bibliographies.

TECHNOLOGY UTILIZATION PUBLICATIONS: Information on technology used by NASA that may be of particular interest in commercial and other non-aerospace applications. Publications include Tech Briefs, Technology Utilization Reports and Notes, and Technology Surveys.

Details on the availability of these publications may be obtained from:

SCIENTIFIC AND TECHNICAL INFORMATION DIVISION

NATIONAL AERONAUTICS AND SPACE ADMINISTRATION

Washington, D.C. 20546